



## OPEN ACCESS

## EDITED BY

Yizhong Huang,  
Nanyang Technological University,  
Singapore

## REVIEWED BY

Helena Maria Rodrigues Gonçalves,  
Chemistry and Technology Network  
(REQUIMTE), Portugal  
Forough Ghasemi,  
Agricultural Biotechnology Research  
Institute of Iran, Iran

## \*CORRESPONDENCE

Qianchuang Sun,  
✉ sunqianchuang@jlu.edu.cn

RECEIVED 11 September 2023

ACCEPTED 27 November 2023

PUBLISHED 08 December 2023

## CITATION

Kan B, Li L, Hou J, Liu S, Tian Z and Sun Q  
(2023), Eu-doped carbon quantum dot as  
a selective probe for visualizing and  
monitoring sulfite in biological systems.  
*Front. Bioeng. Biotechnol.* 11:1292136.  
doi: 10.3389/fbioe.2023.1292136

## COPYRIGHT

© 2023 Kan, Li, Hou, Liu, Tian and Sun.  
This is an open-access article distributed  
under the terms of the [Creative  
Commons Attribution License \(CC BY\)](#).  
The use, distribution or reproduction in  
other forums is permitted, provided the  
original author(s) and the copyright  
owner(s) are credited and that the original  
publication in this journal is cited, in  
accordance with accepted academic  
practice. No use, distribution or  
reproduction is permitted which does not  
comply with these terms.

# Eu-doped carbon quantum dot as a selective probe for visualizing and monitoring sulfite in biological systems

Bo Kan<sup>1</sup>, Li Li<sup>2</sup>, Jiaoyu Hou<sup>3</sup>, Shuyan Liu<sup>4</sup>, Zhenwei Tian<sup>5</sup> and Qianchuang Sun<sup>6\*</sup>

<sup>1</sup>Department of Clinical Laboratory, The Second Hospital of Jilin University, Changchun, Jilin, China, <sup>2</sup>College of Chemistry, Jilin University, Changchun, Jilin, China, <sup>3</sup>Department of Geriatrics, The First Hospital of Jilin University, Changchun, Jilin, China, <sup>4</sup>Department of Ophthalmology, The Second Hospital of Jilin University, Changchun, Jilin, China, <sup>5</sup>Department of Emergency and Critical Care, The Second Hospital of Jilin University, Changchun, Jilin, China, <sup>6</sup>Department of Anesthesiology, The Second Hospital of Jilin University, Changchun, Jilin, China

The detection of  $\text{SO}_3^{2-}$  in complex environments and its visualization at the cellular level are critical for understanding its role in biological processes. In this study, we developed an Eu-doped long-wavelength fluorescent carbon quantum dot (CD2) and investigated the detection mechanism, interference effects and cellular imaging applications of the fluorescent probe CD2. The results show that the addition of  $\text{SO}_3^{2-}$  induces an electronic rearrangement that restores CD2 to its original structure, leading to a rapid increase in fluorescence intensity. Selectivity experiments showed that CD2 has excellent selectivity to  $\text{SO}_3^{2-}$ , with minimal interference from common anions. In addition, CD2 shows good biocompatibility for cellular imaging applications, as evidenced by the high cell viability observed in HeLa cells. Using confocal microscopy, we detected a significant enhancement of red fluorescence in HeLa cells after addition of exogenous  $\text{SO}_3^{2-}$ , demonstrating the potential of CD2 as a probe for monitoring cellular  $\text{SO}_3^{2-}$  levels. These findings highlight the promise of CD2 as a selective  $\text{SO}_3^{2-}$  detection probe in complex environments and its utility in cellular imaging studies. Further studies are necessary to fully exploit the potential of CD2 in various biological and biomedical applications.

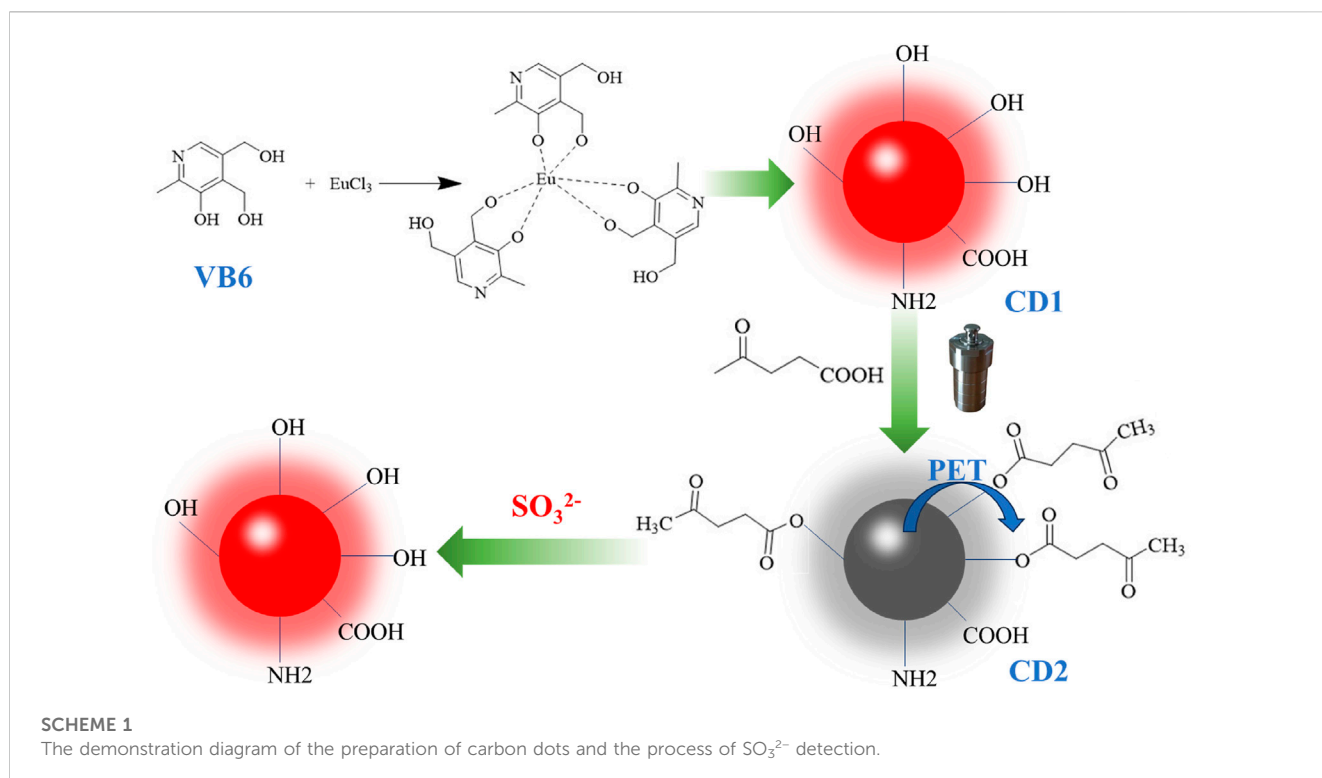
## KEYWORDS

fluorescent probe, selectivity, cellular imaging, sulfite detection, biocompatibility

## 1 Introduction

The detection of intracellular sulfite ions ( $\text{SO}_3^{2-}$ ) is of great significance in the field of biomedical engineering (Tian et al., 2013; Wang et al., 2019; Li Q. et al., 2023). These ions play a critical role in various cellular processes and provide valuable insights into cell function and health. Accurate measurement of sulfite ions is crucial for disease diagnosis, drug development, and understanding the impact of environmental factors on cellular function (Maiti, 2022; Săcărescu et al., 2023).

Within cells, sulfite ions are generated through the oxidation of sulfur-containing amino acids, including cysteine and methionine. These ions are involved in critical intracellular processes such as protein folding, enzyme regulation, and antioxidant defense mechanisms



(Buerman et al., 2021). By modulating cellular signaling pathways, sulfite ions influence gene expression and cellular responses to a wide range of stimuli.

Maintaining an appropriate balance of intracellular sulfite ions is essential for optimal cell health and functionality (Kimura et al., 2019). Imbalances in sulfite ion levels have been associated with the occurrence and progression of several diseases, including cardiovascular disorders, neurodegenerative diseases, and cancer (Zhang et al., 2004). Elevated sulfite concentrations can lead to oxidative stress and cell damage, as excess sulfite can react with reactive oxygen species (ROS) to form toxic compounds (Mitsuhashi et al., 2005). Conversely, abnormally low sulfite ion levels can disrupt cellular processes dependent on sulfite signaling, resulting in impaired antioxidant defenses and compromised cell function (Vincent et al., 2004).

Accurate measurement of intracellular sulfite ion concentrations is instrumental in biomedical research and applications. Sulfite ion detection enables the assessment of sulfite-related diseases, aids in diagnosis, and guides the development of targeted treatment approaches. Additionally, it provides a means to evaluate the impact of potential therapeutic compounds on sulfite-mediated signaling pathways, thereby contributing to advancements in drug development (Danışman et al., 2022; Guo et al., 2023).

Various techniques have been developed for the quantitative detection of intracellular sulfite ion levels (Zhang et al., 2016; Wang P. et al., 2021). Prominent examples include fluorescence-based detection methods (Fu et al., 2022), mass spectrometry analysis (Robbins et al., 2015), and electrochemical biosensors (Badihi-Mossberg et al., 2007). Fluorescent probes allow for real-time visualization and monitoring of sulfite ions within live cells, while mass spectrometry offers high sensitivity and accurate measurements. Electrochemical biosensors provide a simple and rapid detection method suitable for point-of-care applications.

In this study, we propose a novel approach for sulfite ion detection by synthesizing long-wavelength emission fluorescence carbon quantum dots (CD1). These CD1 dots, derived from pyridoxine (vitamin B6) as the carbon source and doped with  $\text{Eu}^{3+}$ , possess exceptional properties such as low toxicity, high biocompatibility, and intense fluorescence (Li et al., 2021; Wareing et al., 2021; Đorđević et al., 2022). To achieve sulfite ion detection, the CD1 dots are subjected to surface modification with pyruvic acid, which quenches their fluorescence through the photoinduced electron transfer (PET) effect (Sun et al., 2019; Allen et al., 2022), rendering them non-fluorescent (hereafter referred to as CD2). Upon reaction with sulfite ions, the removal of pyruvic acid from the surface of CD2 leads to a considerable fluorescence enhancement (Deng et al., 2019; Li W.-B. et al., 2023), enabling highly sensitive detection of sulfite ions (Scheme 1).

Accurate measurement of sulfite ions is vitally important for disease diagnosis, drug development, and understanding the influence of environmental factors on cellular function. The proposed synthesis of long-wavelength emission fluorescence carbon quantum dots, coupled with surface modification, presents a promising approach for achieving sensitive and reliable detection of sulfite ions.

## 2 Materials and methods

### 2.1 Materials and instrumentation

Pyridoxine,  $\text{EuCl}_3$ ,  $\text{Na}_2\text{SO}_3$  and other compounds were unpurified using commercially available standard chemicals. Deionized water used in the experiments was prepared in the laboratory.

Transmission electron microscopy (TEM) and high-resolution TEM (HRTEM) images of the CDs were recorded using a JEOL-

2100F. Fourier transform infrared spectra (FTIR) were obtained using a Nicolet IS-10 FTIR spectrophotometer (Thermo Fisher Scientific). Fourier transform infrared spectra (FTIR) were obtained using a Nicolet IS-10 FTIR spectrophotometer (Thermo Fisher). X-ray photoelectron spectroscopy (XPS) was performed using an X-ray photoelectron spectrometer (AXIS ULTRA DLD). UV-vis absorption spectra were tested on an Agilent Cary 300 Scan. The zeta potential and hydrodynamic size of the samples were determined using a Zetasizer Nano ZS-90 analyzer (Malvern Instruments). Absolute QY and lifetimes were determined using a FLS1000 instrument (Edinburgh Instruments). Fluorescence spectra were obtained using an F97 Pro fluorescence spectrophotometer. Cells were imaged using a Leica TCS-SP8 confocal microscope.

## 2.2 Preparation of the CD1 and CD2

0.5 g of pyridoxine and 0.1 g of  $\text{EuCl}_3$  were dissolved in 40 mL of deionized water and sonicated for 10 min, then the solution was transferred to a 100 mL Teflon-lined stainless-steel autoclave. CD1 solution was obtained after cooling. To the CD1 solution 0.3 g of pyruvic acid was added, stirred well and returned to the reactor for secondary heating for 4 h ( $130^\circ\text{C}$ ). After cooling to room temperature, the reaction product was eluted with a mixture of dichloromethane and methanol (10:1) to give a bright red liquid CD2, which was dried by rotary evaporator. The dried solid was stored at  $4^\circ\text{C}$  in a dark place for future characterization and use.

## 2.3 Detection of $\text{SO}_3^{2-}$

The fluorescence spectra of the samples were recorded after adding different concentrations of  $\text{SO}_3^{2-}$  (1–25  $\mu\text{M}$ ) to the CD2 solution at 20  $\mu\text{g}/\text{mL}$ .

## 2.4 Cytotoxicity assays and cell targeting

The cytotoxicity of CD2 was tested using WST-1. HeLa cells were cultured in 96-well plates at  $10^4$  cells per well. The culture medium consisted of 10% FBS, 100 U/mL penicillin-streptomycin solution and 90% RPMI 1640 medium. After 24 h of incubation, the medium was removed, fresh complete medium containing different concentrations of CD2 (dissolved in DMSO, 5 mg/mL) was added, and the cells were incubated for another 24 h. Finally, the medium was removed, and the cells were rinsed three times with PBS, and the viability of the cells was assessed by the WST-1 assay. Absorption was recorded for all plates using a microplate reader with a wavelength of 450 nm.

To assess the ability of CD2 to detect intracellular  $\text{SO}_3^{2-}$ , HeLa cells were seeded into 35-mm glass-bottomed Petri dishes and cultured at  $37^\circ\text{C}$  in a humidified environment with 5%  $\text{CO}_2$ . After 24 h of incubation, the initial medium was removed, and then 20  $\mu\text{g}/\text{mL}$  of CD2 was added with 2 mL of fresh medium for another 6 h. An additional 25  $\mu\text{M}$  of  $\text{SO}_3^{2-}$  was added to the control experiments. Then, after rinsing the cells three times with PBS, the fluorescence images of the samples were observed using a laser fluorescence confocal microscope.

# 3 Results and discussion

## 3.1 Preparation and characterization of the CDs

CD1 was synthesized through a hydrothermal reaction using VB6 as the carbon source and  $\text{Eu}^{3+}$  as the dopant. CD1 possesses hydroxyl groups on its surface, which can be easily reacted with pyruvic acid through a two-step hydrothermal process. By utilizing the photoinduced electron transfer (PET) effect, the fluorescence of CD1 can be quenched. TEM analysis (Figure 1A) revealed that CD1 exhibited a regular spherical structure with a uniform size and single dispersion in water. The individual particle diameter was determined to be approximately 8 nm, which was further confirmed by DLS measurements (Figure 1B).

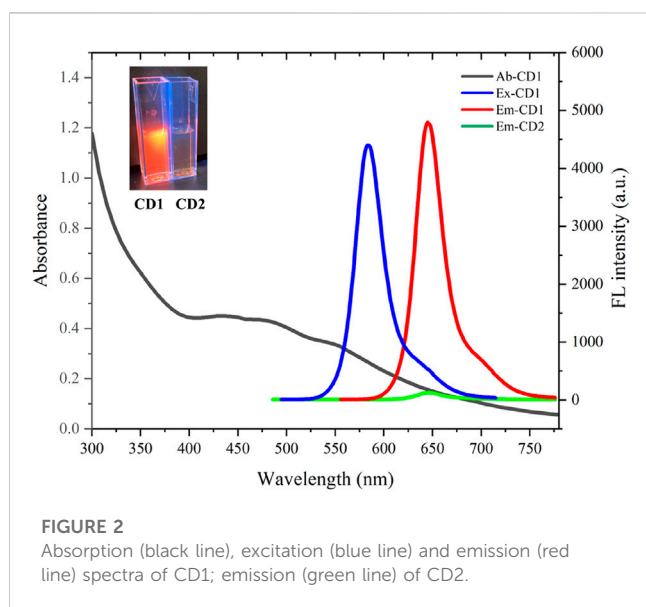
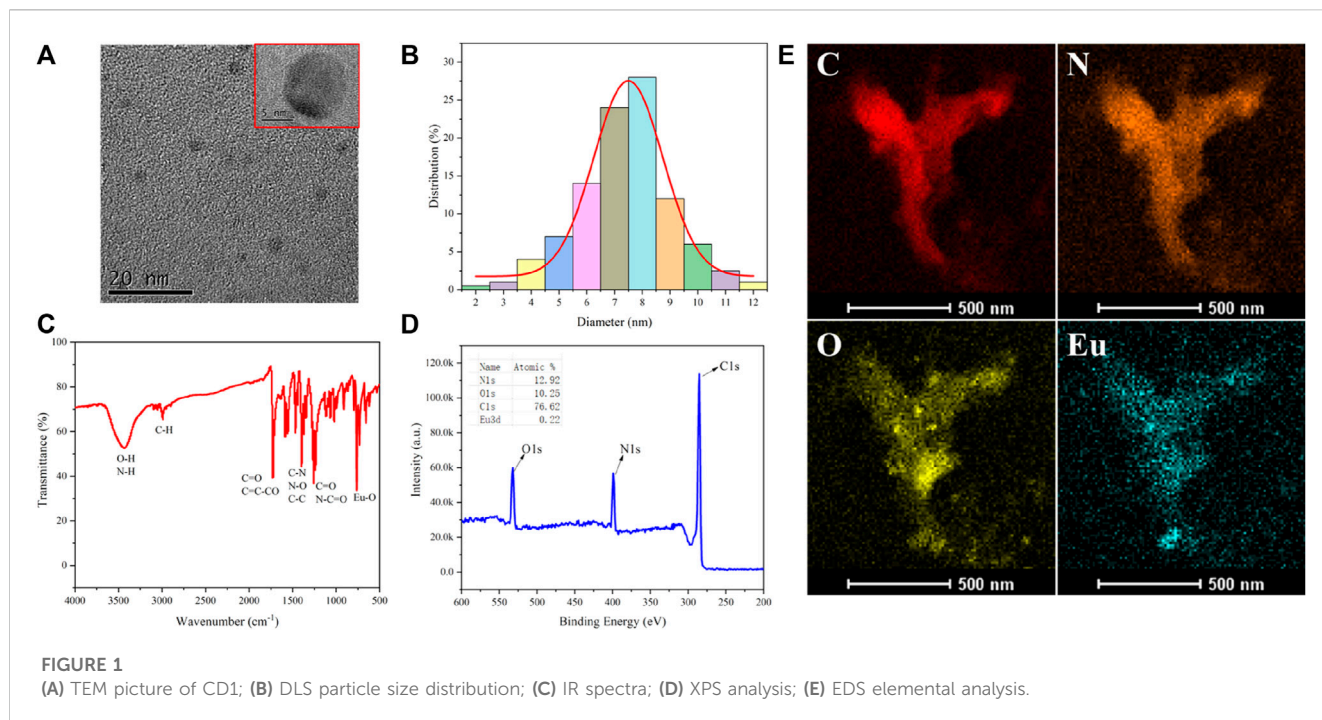
The infrared spectrum of CD1 (Figure 1C) exhibited several characteristic peaks. The peak at around  $750\text{ cm}^{-1}$  originated from the stretching vibration of  $\text{Eu-O}$  bonds, indicating the successful doping of  $\text{Eu}^{3+}$  into the CD1 structure. The peak at  $1,240\text{ cm}^{-1}$  represented the stretching vibration of  $\text{C=O}$  and  $\text{N-C=O}$  bonds, while the peak at  $1,396\text{ cm}^{-1}$  was attributed to the stretching vibration of  $\text{C-N}$  bonds and the bending vibration of  $\text{N-O}$  bonds. The peak at  $1716\text{ cm}^{-1}$  indicated the presence of the  $\text{C=C-CO}$  bending vibration, suggesting the existence of conjugated olefin or aromatic ketone structures in CD1. The peak at  $2,992\text{ cm}^{-1}$  represented the stretching vibration of  $\text{C-H}$  bonds and alkynyl groups. The peak at  $3,423\text{ cm}^{-1}$  corresponded to the stretching vibration of  $\text{O-H}$  and  $\text{N-H}$  bonds, indicating the presence of hydroxyl and amino groups in CD1. X-ray photoelectron spectroscopy (XPS) analysis (Figure 1D) confirmed that CD1 primarily consisted of carbon (C), nitrogen (N), and oxygen (O), with a small amount of Eu (atomic percentage of 0.22%). Furthermore, energy-dispersive X-ray spectroscopy (EDS) elemental analysis (Figure 1E) provided additional confirmation that CD1 was composed of C, N, O, and Eu elements.

Overall, the results demonstrate the successful synthesis of CD1 with a well-defined structure and composition. The incorporation of  $\text{Eu}^{3+}$  as a dopant and the surface modification with pyruvic acid provide CD1 with favorable properties for sulfite ion detection.

## 3.2 Optical properties of carbon dots

The optical properties of the carbon dots are depicted in Figure 2. CD1 shows absorption throughout the visible light range, with a shoulder peak around 470 nm. Its emission peak is located at 650 nm, with an optimal excitation peak at 580 nm. In contrast, CD2 exhibits nearly no fluorescence, with emission intensity even less than 1/50th of CD1's. Thus, CD1 displays bright red fluorescence under excitation, while CD2 exhibits minimal fluorescence (shown in the top left corner of the image). This indicates that the reaction of pyruvic acid with CD1 through the secondary hydrothermal process leads to the quenching of its fluorescence.

The significant contrast in fluorescence between CD1 and CD2 provides the basis for the detection of sulfite ions. The presence of sulfite ions can cause the removal of pyruvic acid from the surface of CD2, restoring its fluorescence. This fluorescence enhancement can be utilized for sensitive and selective detection of sulfite ions. The changes in the optical properties of the carbon dots upon interaction with sulfite ions will allow for the quantification of sulfite ion concentrations in various biological and environmental samples.



### 3.3 Detection of $\text{SO}_3^{2-}$ in solution

The fluorescence-quenched CD2 has been utilized for highly sensitive detection of  $\text{SO}_3^{2-}$ . A certain concentration of CD2 aqueous solution (20  $\mu\text{g}/\text{mL}$ ) was prepared, and different concentrations of  $\text{SO}_3^{2-}$  (ranging from 1–25  $\mu\text{M}$ ) were added. As the concentration of  $\text{SO}_3^{2-}$  increased, the fluorescence intensity of the solution rapidly intensified. Even with the addition of 5  $\mu\text{M}$   $\text{SO}_3^{2-}$ , the fluorescence intensity increased by more than six times. When 25  $\mu\text{M}$   $\text{SO}_3^{2-}$  was added, the intensity increase slowed down, eventually reaching over 30 times the initial intensity (Figure 3A).

The fluorescence of the CD2 solution enhanced almost instantaneously upon the addition of  $\text{SO}_3^{2-}$ , reaching stability within 2 min (Figure 3B). This indicates the high sensitivity of CD2 to  $\text{SO}_3^{2-}$  and its potential as a rapid detection probe. Figure 3C displays the relationship between  $\text{SO}_3^{2-}$  concentration and the fluorescence intensity of the CD2 solution. It shows good linearity within the range of 1–20  $\mu\text{M}$  ( $R^2 = 0.998$ ), following equation  $F/F_0 - 1 = 0.429 + 1.968x$ , where  $F$  represents the fluorescence intensity of the CD2 solution after the addition of  $\text{SO}_3^{2-}$ , and  $F_0$  represents the initial fluorescence intensity of the CD2 solution.

To determine the limit of detection (LOD), the equation  $\text{LOD} = 3\sigma/S$  was used, in which  $\sigma$  is the standard deviation of the fluorescence intensity of the CD2 solution without the addition of  $\text{SO}_3^{2-}$ , and  $S$  is the slope of the fitting line. Based on this calculation, the LOD was estimated to be approximately 0.15  $\mu\text{M}$ , which is lower than both electrochemical and colorimetric methods, and at the same level as other fluorescent probes (Table 1). And the limit of quantification (LOQ) was calculated as 0.5  $\mu\text{M}$ .

Meanwhile, the effect of pH on the detection process was considered. The probe CD2 itself is almost non-fluorescent at different pH values, and the detection of sulfites remains stable in the pH range of 7.0–10.0 (Figure 3D). The pH values of human sulfite metabolism sites are mainly between 7.0 and 8.5 (e.g., brain 7.1, heart 7.0–7.4, bile 7.8, liver 7.2, blood 7.3–7.45, pancreatic secretion 8.0–8.3, and bone 7.4) (Hashim et al., 2011; Yue et al., 2017), and therefore, CD2 is almost sufficient for the detection.

These results suggest that the quenching and recovery of fluorescence in CD2 can be effectively applied for the sensitive and selective detection of sulfite ions in solution. The high sensitivity, rapid response, and low limit of detection make CD2 a promising candidate for sulfite ion detection in various applications.

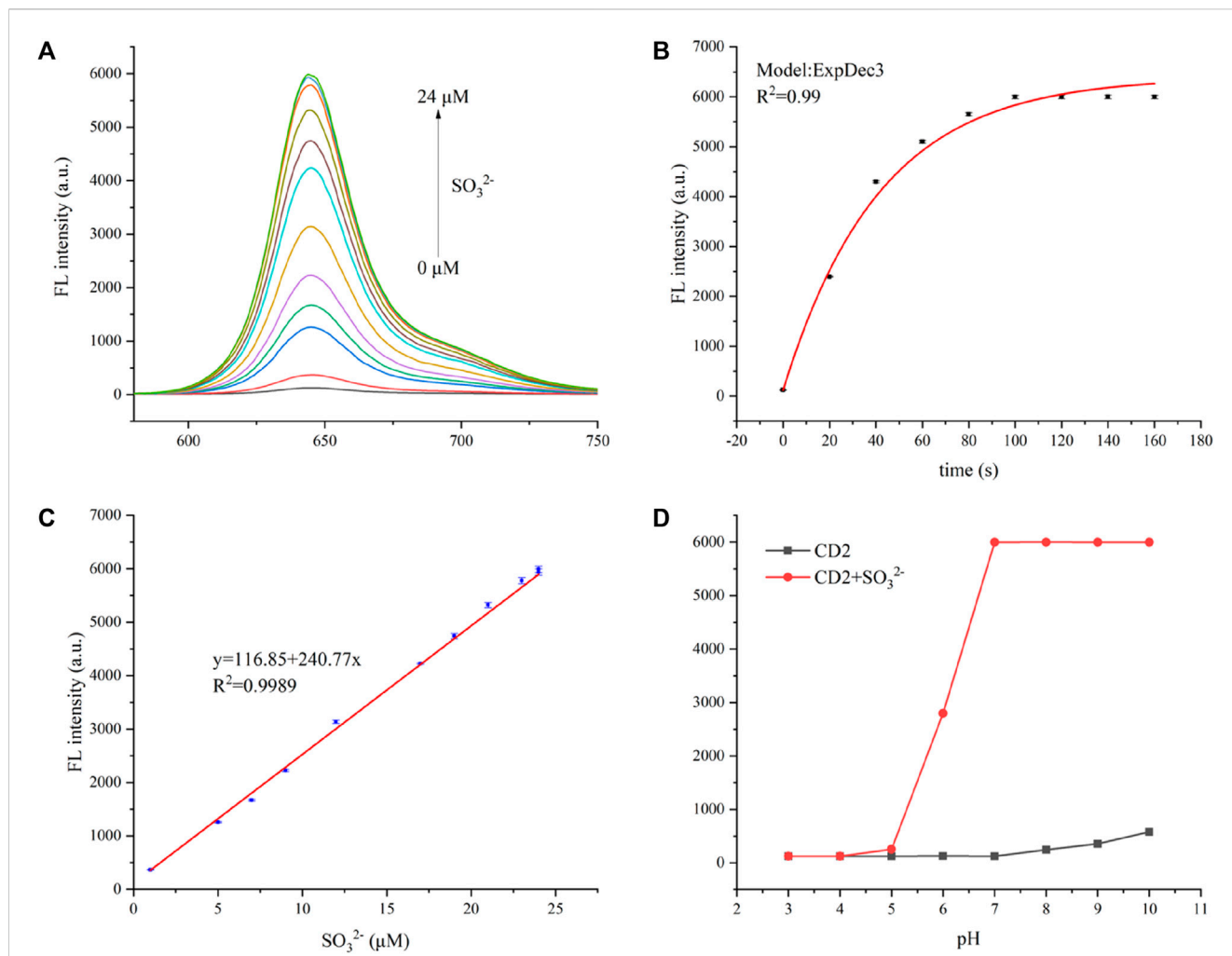


**FIGURE 3**

(A) Fluorescent spectra of the CD2 solution with the addition of different concentrations of  $\text{SO}_3^{2-}$  at an excitation wavelength of 580 nm. (B) Time-dependent fluorescence intensity spectra of CD2 (20  $\mu\text{g}/\text{mL}$ ) at 650 nm in the presence of  $\text{SO}_3^{2-}$  (25  $\mu\text{M}$ ). (C) The linear relationship between (F0/F−1) and the concentration of  $\text{SO}_3^{2-}$  over the range of 1–25  $\mu\text{M}$ . (D) The fluorescence intensity of CD2 (20  $\mu\text{g}/\text{mL}$ ) at 650 nm in the absence and presence of  $\text{SO}_3^{2-}$  (25  $\mu\text{M}$ ) in various pH conditions (3.0–10.0). Incubation temperature: 37°C.

**TABLE 1 Comparison with existing  $\text{SO}_3^{2-}$  detection methods.**

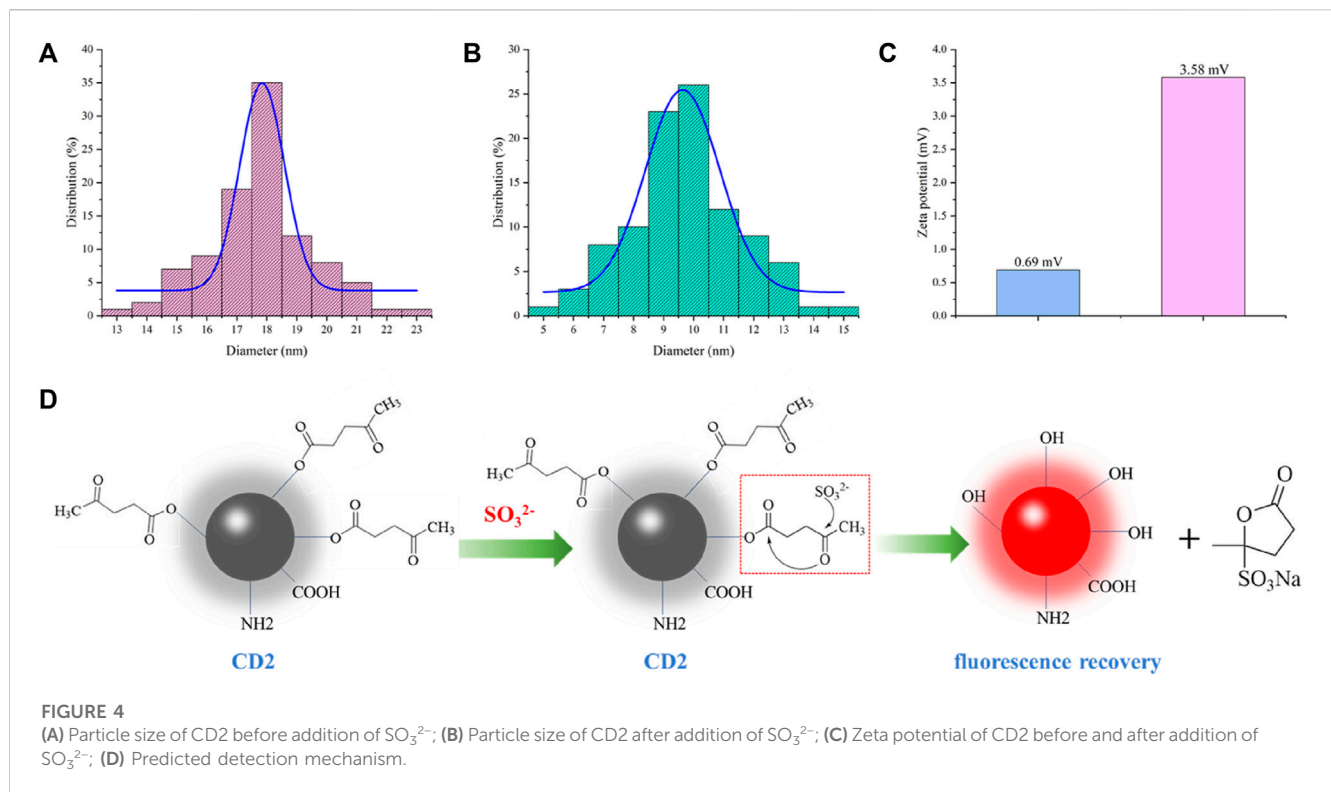
| Materials                           | Method                 | Linear range          | LOD ( $\mu\text{M}$ ) | References                  |
|-------------------------------------|------------------------|-----------------------|-----------------------|-----------------------------|
| Nanostructured copper-salen film    | electrochemical sensor | 4–69 $\mu\text{M}$    | 1.2                   | Dadamos and Teixeira (2009) |
| $\text{Ag}_2\text{O}$ nanoparticles | colorimetric detection | 100–500 $\mu\text{M}$ | 10                    | Lu et al. (2015)            |
| rhodamine-derivated probe           | fluorescent            | 0–80 $\mu\text{M}$    | 0.6                   | Wang et al. (2021a)         |
| ratiometric fluorescent probe       | fluorescent            | 0–100 $\mu\text{M}$   | 0.57                  | Venkatachalam et al. (2020) |
| Carbon dots                         | fluorescent            | 0–25 $\mu\text{M}$    | 0.15                  | This work                   |

### 3.4 Mechanisms for the detection of $\text{SO}_3^{2-}$

To gain insight into the detection mechanism of  $\text{SO}_3^{2-}$ , we conducted tests on the particle size (Figures 4A, B) and surface potential (Figure 4C) of the solution before and after the reaction. Upon the addition of  $\text{SO}_3^{2-}$ , the particle size of CD2 decreased from approximately 18 nm to around 10 nm, which is close to the average particle size of CD1. Additionally, the

surface potential increased from +0.69 mV to +3.58 mV. These observations provide valuable information for proposing a possible detection mechanism for  $\text{SO}_3^{2-}$  (Figure 4D).

In the two-step hydrothermal method, pyruvic acid is chemically modified onto the surface of CD1 through an ester linkage, resulting in the formation of CD2. The fluorescence of CD2 is quenched due to the photoinduced electron transfer (PET) effect. Upon the addition of  $\text{SO}_3^{2-}$



to the CD2 solution, the oxygen atom in  $\text{SO}_3^{2-}$  interacts with the aldehyde group of pyruvic acid. This interaction leads to electron rearrangement and the formation of a transition state involving the oxygen atom on the carbonyl carbon of the ester moiety. Finally, the transition state decomposes, breaking the ester bond and generating a sulfonate-substituted furanone derivative. As a result, CD2 is restored to the structure of CD1, and the fluorescence intensity rapidly increases.

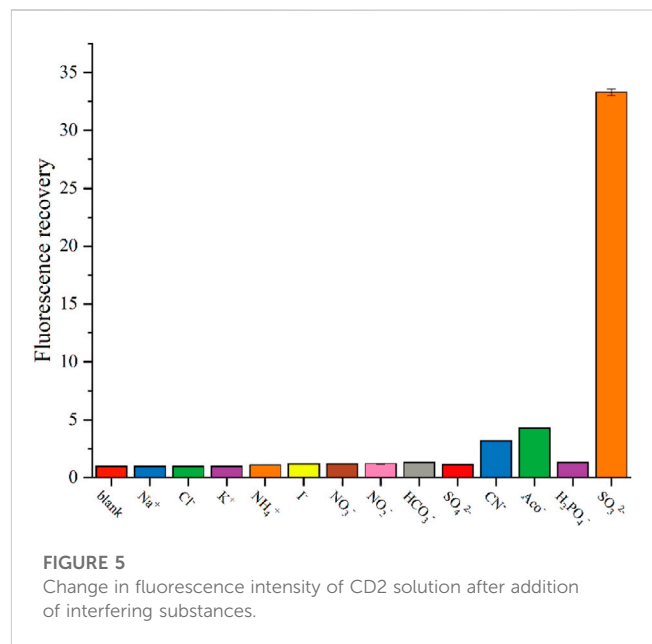
Further investigations are necessary to fully understand the detailed mechanism of  $\text{SO}_3^{2-}$  detection using CD2. Nevertheless, these preliminary findings provide important insights and a plausible explanation for the observed fluorescence enhancement upon the addition of  $\text{SO}_3^{2-}$  in the CD2 solution.

### 3.5 Interference experiments

To assess the interference of other ions in the detection process of  $\text{SO}_3^{2-}$ , we conducted experiments to test the effects of commonly encountered anions, such as  $\text{Cl}^-$ ,  $\text{I}^-$ ,  $\text{NO}_3^-$ ,  $\text{HCO}_3^-$ ,  $\text{SO}_4^{2-}$ ,  $\text{AcO}^-$ ,  $\text{CN}^-$ , and  $\text{H}_2\text{PO}_4^-$ , on the fluorescence of the CD2 solution. Figure 5 illustrates the results obtained.

Upon adding 25  $\mu\text{M}$  of  $\text{Na}^+$ ,  $\text{K}^+$ ,  $\text{NH}_4^+$ ,  $\text{Cl}^-$ ,  $\text{I}^-$ ,  $\text{NO}_3^-$ ,  $\text{HCO}_3^-$ ,  $\text{SO}_4^{2-}$ , and  $\text{H}_2\text{PO}_4^-$  individually, the fluorescence intensity of the CD2 solution remained almost unchanged. Most of common cations and anions do not interfere with the detection, consistent with other research (Wang K. et al., 2021). Only  $\text{CN}^-$  and  $\text{AcO}^-$  caused a slight increase in fluorescence intensity, approximately three times higher. However, when comparing this increase to the 30-fold amplification observed with  $\text{SO}_3^{2-}$ , it is negligible.

These findings indicate that CD2 exhibits exceptional selectivity for  $\text{SO}_3^{2-}$ . The lack of interference from commonly encountered



anions suggests that the detection of  $\text{SO}_3^{2-}$  in complex environments holds promising potential for various applications.

### 3.6 Toxicity assays and cellular imaging applications of CD2

To assess the feasibility of using CD2 for cell imaging, a cell viability assay was conducted using the WST-1 reagent. The results

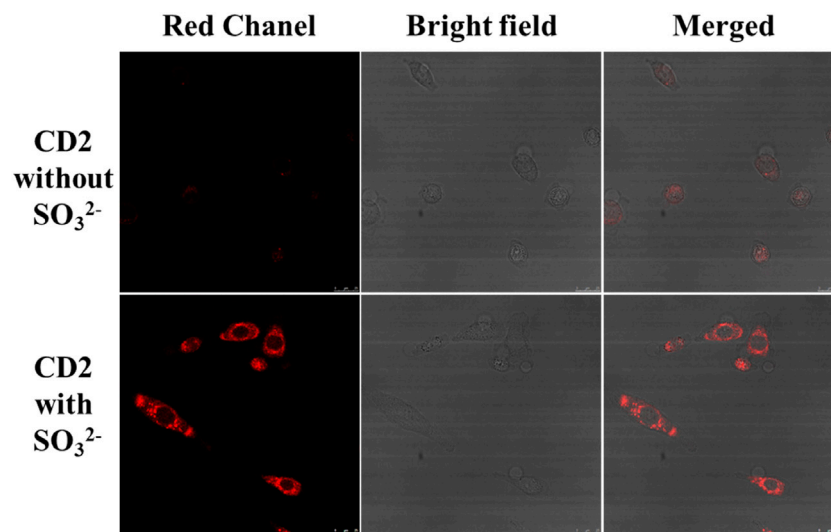


**FIGURE 6**

Changes in fluorescence intensity of HeLa cells before and after addition of  $\text{SO}_3^{2-}$  (scale bar: 25  $\mu\text{m}$ ).

demonstrated that the cell viability of HeLa cells remained above 90% when different concentrations of CD2 (ranging from 0 to 100  $\mu\text{g}/\text{mL}$ ) were added. This indicates that CD2 exhibits good biocompatibility for cell imaging purposes.

Subsequently, the potential application of CD2 in cell imaging was further explored using a Leica SP8 confocal microscope. The fluorescence changes of CD2 were studied at the cellular level by introducing exogenous  $\text{SO}_3^{2-}$  into HeLa cells. Figure 6 illustrates the results obtained. As shown, a significant enhancement of red fluorescence was observed in HeLa cells following the addition of 20  $\mu\text{M}$  of  $\text{SO}_3^{2-}$ . This observation suggests that CD2 can effectively detect the level of  $\text{SO}_3^{2-}$  in HeLa cells and has the potential to serve as a probe for cellular imaging applications.

These findings demonstrate the potential of CD2 for cellular imaging and highlight its ability to detect and monitor the levels of  $\text{SO}_3^{2-}$  in living cells.

## 4 Conclusion

In conclusion, our study investigated the detection mechanism, interference effects, and potential applications of CD2 in the detection of  $\text{SO}_3^{2-}$ . The results indicated that CD2 exhibits a promising detection mechanism, where the addition of  $\text{SO}_3^{2-}$  leads to electron rearrangement and the restoration of CD2 to its original structure, resulting in a rapid increase in fluorescence intensity. Furthermore, CD2 demonstrated excellent selectivity for  $\text{SO}_3^{2-}$ , as evidenced by minimal interference from commonly encountered anions.

To assess the biocompatibility of CD2 for cellular imaging applications, a cell viability assay exhibited high cell viability when different concentrations of CD2 were added to HeLa cells. This indicates that CD2 has good biocompatibility for cell imaging. Moreover, cellular imaging experiments using CD2 revealed its ability to detect and monitor the levels of  $\text{SO}_3^{2-}$  in living cells, as manifested by a significant enhancement of red fluorescence upon the addition of exogenous  $\text{SO}_3^{2-}$  to HeLa cells.

Overall, these findings suggest that CD2 holds promise as a probe for the detection of  $\text{SO}_3^{2-}$  in complex environments and its application in cellular imaging. Further studies are warranted to explore the full potential and specific mechanisms of CD2 in various applications.

## Data availability statement

The original contributions presented in the study are included in the article/supplementary material, further inquiries can be directed to the corresponding author.

## Author contributions

BK: Conceptualization, Formal Analysis, Investigation, Methodology, Writing–original draft, Writing–review and editing. LL: Conceptualization, Formal Analysis, Writing–review and editing. JH: Conceptualization, Data curation, Formal Analysis, Writing–original draft. SL: Data curation, Formal Analysis, Software, Writing–original draft. ZT: Data curation, Investigation, Software, Writing–original draft. QS: Conceptualization, Funding acquisition, Writing–review and editing.

## Funding

The authors declare that no financial support was received for the research, authorship, and/or publication of this article.

## Conflict of interest

The authors declare that the research was conducted in the absence of any commercial or financial relationships that could be construed as a potential conflict of interest.

## Publisher's note

All claims expressed in this article are solely those of the authors and do not necessarily represent those of their affiliated

organizations, or those of the publisher, the editors and the reviewers. Any product that may be evaluated in this article, or claim that may be made by its manufacturer, is not guaranteed or endorsed by the publisher.

## References

- Allen, A. R., Noten, E. A., and Stephenson, C. R. J. (2022). Aryl transfer strategies mediated by photoinduced electron transfer. *Chem. Rev.* 122 (2), 2695–2751. doi:10.1021/acs.chemrev.1c00388
- Badihi-Mossberg, M., Buchner, V., and Rishpon, J. (2007). Electrochemical biosensors for pollutants in the environment. *Electroanal. Environ.* 19 (19–20), 2015–2028. doi:10.1002/elan.200703946
- Buerman, E. C., Worobo, R. W., and Padilla-Zakour, O. I. (2021). High pressure processing of heat and pressure resistant fungi as affected by pH, water activity, sulfites, and dimethyl dicarbonate in a diluted apple juice concentrate. *Food Control.* 120, 107551. doi:10.1016/j.foodcont.2020.107551
- Dadamos, T. R. L., and Teixeira, M. F. S. (2009). Electrochemical sensor for sulfite determination based on a nanostructured copper-salen film modified electrode. *Electrochimica Acta* 54 (19), 4552–4558. doi:10.1016/j.electacta.2009.03.045
- Danışman, B., Akçay, G., Gökçek-Saraç, Ç., Kantar, D., Aslan, M., and Derin, N. (2022). The role of acetylcholine on the effects of different doses of sulfite in learning and memory. *Neurochem. Res.* 47 (11), 3331–3343. doi:10.1007/s11064-022-03684-z
- Deng, K., Wang, L., Xia, Q., Liu, R., and Qu, J. (2019). A turn-on fluorescent chemosensor based on aggregation-induced emission for cyanide detection and its bioimaging applications. *Sensors Actuators B Chem.* 296, 126645. doi:10.1016/j.snb.2019.126645
- Dorđević, L., Arcudi, F., Cacioppo, M., and Prato, M. (2022). A multifunctional chemical toolbox to engineer carbon dots for biomedical and energy applications. *Nat. Nanotechnol.* 17 (2), 112–130. doi:10.1038/s41565-021-01051-7
- Fu, Y., Zhang, X., Liu, J., Qian, G., Xu, Z. P., and Zhang, R. (2022). Fluorescence detection and imaging of intracellular sulphite using a remote light activatable photochromic nanoprobe. *J. Mater. Chem. B* 10 (17), 3366–3374. doi:10.1039/D2TB00021K
- Guo, J., Wang, W., Xie, S., Zhang, Y., Li, J., Xu, J., et al. (2023). Performance and mechanism of sulfite mediated oxidation of organic contaminants using iron(III) titanium oxide as catalyst. *J. Environ. Chem. Eng.* 11 (5), 110449. doi:10.1016/j.jece.2023.110449
- Hashim, A. I., Zhang, X., Wojtkowiak, J. W., Martinez, G. V., and Gillies, R. J. (2011). Imaging pH and metastasis. *Imaging P. H. metastasis* 24 (6), 582–591. doi:10.1002/nbm.1644
- Kimura, Y., Shibuya, N., and Kimura, H. (2019). Sulfite protects neurons from oxidative stress. *Br. J. Pharmacol.* 176 (4), 571–582. doi:10.1111/bph.14373
- Li, Q., Yan, S., Song, H., Su, Y., Sun, M., and Lv, Y. (2023a). A simple and stable chemiluminescence resonance energy transfer system based on Ce(IV)-MOFs for detection of sulfite. *Sensors Actuators B Chem.* 376, 132990. doi:10.1016/j.snb.2022.132990
- Li, S., Li, L., Tu, H., Zhang, H., Silvester, D. S., Banks, C. E., et al. (2021). The development of carbon dots: from the perspective of materials chemistry. *Mater. Today* 51, 188–207. doi:10.1016/j.mattod.2021.07.028
- Li, W.-B., Wu, Y., Zhong, X.-F., Chen, X.-H., Liang, G., Ye, J.-W., et al. (2023b). Fluorescence enhancement of a metal-organic framework for ultra-efficient detection of trace benzene vapor. *Angew. Chem. Int. Ed. Engl.* 62 (24), e202303500. doi:10.1002/anie.202303500
- Lu, W., Shu, J., Wang, Z., Huang, N., and Song, W. (2015). The intrinsic oxidase-like activity of Ag<sub>2</sub>O nanoparticles and its application for colorimetric detection of sulfite. *Mater. Lett.* 154, 33–36. doi:10.1016/j.matlet.2015.04.051
- Maiti, B. K. (2022). Cross-talk between (Hydrogen)Sulfite and metalloproteins: impact on human health. *Impact Hum. Health* 28 (23), e202104342. doi:10.1002/chem.202104342
- Mitsuhashi, H., Yamashita, S., Ikeuchi, H., Kuroiwa, T., Kaneko, Y., Hiromura, K., et al. (2005). Oxidative stress-dependent conversion of hydrogen sulfide to sulfite by activated neutrophils. *Shock* 24 (6), 529–534. doi:10.1097/01.shk.0000183393.83272.de
- Robbins, K. S., Shah, R., MacMahon, S., and de Jager, L. S. (2015). Development of a liquid chromatography–tandem mass spectrometry method for the determination of sulfite in food. *J. Agric. Food Chem.* 63 (21), 5126–5132. doi:10.1021/jf505525z
- Săcărescu, L., Chibac-Scutaru, A.-L., Roman, G., Săcărescu, G., and Simionescu, M. (2023). Selective detection of metal ions, sulfites and glutathione with fluorescent pyrazolines: a review. *Environ. Chem. Lett.* 21 (1), 561–596. doi:10.1007/s10311-022-01508-8
- Sun, W., Li, M., Fan, J., and Peng, X. (2019). Activity-based sensing and theranostic probes based on photoinduced electron transfer. *Accounts Chem. Res.* 52 (10), 2818–2831. doi:10.1021/acs.accounts.9b00340
- Tian, H., Qian, J., Sun, Q., Bai, H., and Zhang, W. (2013). Colorimetric and ratiometric fluorescent detection of sulfite in water via cationic surfactant-promoted addition of sulfite to  $\alpha,\beta$ -unsaturated ketone. *Anal. Chim. Acta* 788, 165–170. doi:10.1016/j.aca.2013.06.020
- Venkatachalam, K., Asaithambi, G., Rajasekaran, D., and Periasamy, V. (2020). A novel ratiometric fluorescent probe for “naked-eye” detection of sulfite ion: applications in detection of biological SO<sub>3</sub><sup>2-</sup> ions in food and live cells. *Spectrochimica Acta Part A Mol. Biomol. Spectrosc.* 228, 117788. doi:10.1016/j.saa.2019.117788
- Vincent, A. S., Lim, B. G., Tan, J., Whiteman, M., Cheung, N. S., Halliwell, B., et al. (2004). Sulfite-mediated oxidative stress in kidney cells. *Kidney Int.* 65 (2), 393–402. doi:10.1111/j.1523-1755.2004.00391.x
- Wang, K., Wang, W., Chen, S.-Y., Guo, J.-C., Li, J.-H., Yang, Y.-S., et al. (2021a). A novel Near-Infrared rhodamine-derived turn-on fluorescence probe for sensing SO<sub>3</sub><sup>2-</sup> detection and their bio-imaging *in vitro* and *in vivo*. *Dyes Pigments* 188, 109229. doi:10.1016/j.dyepig.2021.109229
- Wang, K.-N., Zhu, Y., Xing, M., Cao, D., Guan, R., Zhao, S., et al. (2019). Two-photon fluorescence probes for mitochondria imaging and detection of sulfite/bisulfite in living cells. *Sensors Actuators B Chem.* 295, 215–222. doi:10.1016/j.snb.2019.05.077
- Wang, P., Zhang, Y., Liu, Y., Pang, X., Liu, P., Dong, W.-F., et al. (2021b). Starch-based carbon dots for nitrite and sulfite detection. *Front. Chem.* 9, 782238. doi:10.3389/fchem.2021.782238
- Wareing, T. C., Gentile, P., and Phan, A. N. (2021). Biomass-based carbon dots: current development and future perspectives. *ACS Nano* 15 (10), 15471–15501. doi:10.1021/acsnano.1c03886
- Yue, Y., Huo, F., Lee, S., Yin, C., and Yoon, J. (2017). A review: the trend of progress about pH probes in cell application in recent years. *Analyst* 142 (1), 30–41. doi:10.1039/C6AN01942K
- Zhang, L.-J., Wang, Z.-Y., Cao, X.-J., Liu, J.-T., and Zhao, B.-X. (2016). An effective ICT-based and ratiometric fluorescent probe for sensing sulfite. *Sensors Actuators B Chem.* 236, 741–748. doi:10.1016/j.snb.2016.06.055
- Zhang, X., Vincent, A. S., Halliwell, B., and Wong, K. P. (2004). A mechanism of sulfite neurotoxicity: direct inhibition of glutamate dehydrogenase. *J. Biol. Chem.* 279 (41), 43035–43045. doi:10.1074/jbc.M402759200